



HAL
open science

Meridional Contrasts in Productivity Changes Driven by the Opening of Drake Passage

Jean-Baptiste Ladant, Yannick Donnadieu, Laurent Bopp, Caroline Lear,
Paul Wilson

► **To cite this version:**

Jean-Baptiste Ladant, Yannick Donnadieu, Laurent Bopp, Caroline Lear, Paul Wilson. Meridional Contrasts in Productivity Changes Driven by the Opening of Drake Passage. *Paleoceanography*, 2018, 33 (3), pp.302 - 317. 10.1002/2017PA003211 . hal-01806795

HAL Id: hal-01806795

<https://hal.science/hal-01806795>

Submitted on 26 Oct 2020

HAL is a multi-disciplinary open access archive for the deposit and dissemination of scientific research documents, whether they are published or not. The documents may come from teaching and research institutions in France or abroad, or from public or private research centers.

L'archive ouverte pluridisciplinaire **HAL**, est destinée au dépôt et à la diffusion de documents scientifiques de niveau recherche, publiés ou non, émanant des établissements d'enseignement et de recherche français ou étrangers, des laboratoires publics ou privés.

Online Research @ Cardiff

This is an Open Access document downloaded from ORCA, Cardiff University's institutional repository: <http://orca.cf.ac.uk/109934/>

This is the author's version of a work that was submitted to / accepted for publication.

Citation for final published version:

Ladant, Jean-Baptiste, Donnadieu, Yannick, Bopp, Laurent, Lear, Caroline and Wilson, Paul A. 2018. Meridional contrasts in productivity changes driven by the opening of Drake Passage. *Paleoceanography and Paleoclimatology* 33 (3) , pp. 302-317. 10.1002/2017PA003211 file

Publishers page: <http://dx.doi.org/10.1002/2017PA003211>
<<http://dx.doi.org/10.1002/2017PA003211>>

Please note:

Changes made as a result of publishing processes such as copy-editing, formatting and page numbers may not be reflected in this version. For the definitive version of this publication, please refer to the published source. You are advised to consult the publisher's version if you wish to cite this paper.

This version is being made available in accordance with publisher policies. See <http://orca.cf.ac.uk/policies.html> for usage policies. Copyright and moral rights for publications made available in ORCA are retained by the copyright holders.



1 Meridional contrasts in productivity changes driven by the opening of

2 Drake Passage

3

4 Jean-Baptiste Ladant^{1,2,3*}, Yannick Donnadieu^{1,4}, Laurent Bopp^{2,3}, Caroline H.

5 Lear⁵, Paul A. Wilson⁶

6

7 *Corresponding author. Email: jbladant@gmail.com

8 ¹Laboratoire des Sciences du Climat et de l'Environnement, LSCE-IPSL, CEA / CNRS /

9 UVSQ, Université Paris-Saclay, Gif-sur-Yvette, France.

10 ²Ecole Normale Supérieure, Département de Géosciences, Paris, France.

11 ³LMD / IPSL, CNRS / ENS / Ecole Polytechnique / UPMC, Paris, France.

12 ⁴Aix Marseille Université, CNRS, IRD, Coll. France, CEREGE, Aix-en-Provence, France.

13 ⁵School of Earth and Ocean Sciences, Cardiff University, Cardiff, UK.

14 ⁶Ocean and Earth Science, National Oceanography Centre Southampton, University of

15 Southampton, Southampton, UK.

16

17 **Keypoints**

18 • Productivity changes following Drake Passage opening are explored using the IPSL model
19 and compared with data from the late Eocene and early Oligocene.

20 • Drake Passage opening drives a decrease in productivity in the low latitudes and spatially
21 heterogeneous patterns in the high latitudes.

22 • Agreement between proxy records and model results indicate that Drake Passage opening
23 has driven part of the late Eocene productivity changes.

24

25 **Abstract**

26 Changes in atmospheric pCO₂ are widely suggested to have played a major role in both the
27 long-term deterioration of Cenozoic climate and many superimposed rapid climate
28 perturbations such as the pivotal Eocene-Oligocene transition. Changes in marine productivity
29 affecting the biological oceanic carbon pump represent one possible cause of past CO₂
30 variability. Here, we explore the relationship between ocean gateway change and marine
31 biogeochemistry. Specifically, we use a fully coupled atmosphere-ocean-biogeochemical
32 model (IPSL-CM5A) to examine global ocean paleoproductivity changes in response to the
33 opening of Drake Passage. In our simulations, we find that Drake Passage opening yields a
34 spatially uniform decrease in primary productivity in the low latitude oceans while the high
35 latitude response is more spatially heterogeneous. Mechanistically, the low latitude
36 productivity decrease is a consequence of a fundamental reorganization of ocean circulation
37 when Drake Passage opens driven by the isolation of the Southern Ocean from low latitude
38 water masses. Nutrient-depletion in the low latitudes is driven by a marked decrease in the
39 intensity of deep convection in the Southern Ocean, which drives the accumulation of
40 nutrients at depth and their depletion in the intermediate and upper ocean, especially away
41 from sites of subduction. In the high latitudes, the onset of the Antarctic Circumpolar Current
42 in the model exerts a strong control both on nutrient availability but also on regions of deep-
43 water formation. The qualitative agreement between geographically diverse long-term
44 paleoproductivity records and the simulated variations suggests that Drake Passage opening
45 may contribute to the long-term paleoproductivity signal.

46

47

48

49

50 **Introduction**

51 Tectonic opening of Southern Ocean gateways constitutes one of the most
52 fundamental changes in Cenozoic boundary conditions because of the capacity to alter global
53 ocean circulation and climate [*Barker and Burrell, 1977; Kennett, 1977*]. In a seminal paper,
54 *Kennett [1977]* proposed that the opening of these gateways (Drake and Tasman Passages) to
55 deep circulation was instrumental in initiating sustained Antarctic glaciation. This sequence of
56 events is suggested to have initiated during the late Eocene [*Matthews and Poore, 1980;*
57 *Miller et al., 1991; Lear et al., 2000; Stickley et al., 2004; Lagabrielle et al., 2009*], although
58 debate is ongoing about the timing of full gateway opening to a deep and wide current system
59 [*Barker et al., 2007; Katz et al., 2011; Scher et al., 2015*]. This appealing hypothesis suggests
60 that the opening of Drake Passage (DP) and of the Tasman gateway would have engendered
61 the onset of an Antarctic Circumpolar Current (ACC), thermally isolating the Antarctic
62 continent from water masses sourced in the lower latitudes and permitting the growth of an
63 extensive Antarctic ice sheet (AIS). However, this ocean gateway hypothesis has
64 subsequently lost some ground because the results of numerical model experiments have been
65 unable to robustly demonstrate that the sole climatic impact of DP (or Tasman gateway)
66 opening was sufficient to initiate the glaciation [*Mikolajewicz et al., 1993; DeConto and*
67 *Pollard, 2003; Huber and Nof, 2006; Sijp et al., 2011; Goldner et al., 2014*]. Instead,
68 modelling studies have pointed to a CO₂ decline as the primary driver of AIS initiation
69 through atmospheric radiative cooling [*Mikolajewicz et al., 1993; DeConto and Pollard,*
70 *2003; Huber et al., 2004*]. The remarkable match between observations [*Coxall et al., 2005;*
71 *Coxall and Wilson, 2011*] and model predictions [*DeConto and Pollard, 2003; Ladant et al.,*
72 *2014*] of the structure of the deep sea oxygen isotope record across the Eocene-Oligocene
73 transition (EOT) and paleo-CO₂ reconstructions for this interval [*Pearson et al., 2009; Pagani*
74 *et al., 2011; Heureux and Rickaby, 2015*] lend support to the CO₂ hypothesis. Yet these CO₂

75 reconstructions are far from well-developed and the influence of ocean gateway opening and
76 CO₂ forcing need not be mutually exclusive [*Egan et al.*, 2013; *Lear and Lunt*, 2016;
77 *Elsworth et al.*, 2017].

78 There exists a rich literature documenting long-term changes in oceanic carbon
79 cycling associated with Cenozoic climate deterioration including across the pivotal EOT
80 thanks to scientific ocean drilling [e.g., *Siesser*, 1995; *Schumacher and Lazarus*, 2004; *Faul*
81 *and Delaney*, 2010; *Griffith et al.*, 2010; *Coxall and Wilson*, 2011; *Pälike et al.*, 2012; *Egan*
82 *et al.*, 2013; *Moore et al.*, 2014; *Plancq et al.*, 2014; *Villa et al.*, 2014]. Paleoproductivity
83 reconstructions from the data – taken here to mean export production of organic matter to the
84 deep ocean since most paleo data studies inherently quantify export production rather than
85 primary productivity – display spatially heterogeneous long-term variations between the late
86 Eocene and the Oligocene (Table 1). Data from the northern high-latitudes are lacking but
87 records from the southern high-latitudes generally document paleoproductivity increases from
88 the Eocene into the Oligocene [*Schumacher and Lazarus*, 2004; *Plancq et al.*, 2014; *Villa et*
89 *al.*, 2014] while the low latitudes record a general decrease [*Schumacher and Lazarus*, 2004;
90 *Griffith et al.*, 2010; *Moore et al.*, 2014].

91 Numerical modelling studies have investigated the role of DP opening on global ocean
92 circulation and climate with spatially resolved Earth system models [*Mikolajewicz et al.*,
93 1993; *Toggweiler and Bjornsson*, 2000; *Sijp and England*, 2004; *Sijp et al.*, 2009; *Zhang et*
94 *al.*, 2010; *Sijp et al.*, 2011; *Yang et al.*, 2014; *Fyke et al.*, 2015; *England et al.*, 2017]. In
95 contrast, modelling of ocean biogeochemical changes across the late Eocene and Oligocene
96 has been limited. Most work of this type has been undertaken using either numerical box
97 models focusing specifically on the Eocene-Oligocene Transition itself [*Zachos and Kump*,
98 2005; *Merico et al.*, 2008; *Armstrong McKay et al.*, 2016] or using the UVic earth system
99 model of intermediate complexity (EMIC) integrating a biogeochemical component [*Pagani*

100 *et al.*, 2011; *Fyke et al.*, 2015]. Box models are powerful tools to investigate the credibility of
101 competing hypotheses at the global scale but they cannot be used to confront localized
102 paleoproductivity reconstructions. On the other hand, results from experiments using the
103 UVic EMIC suggest that the successive opening of DP and of the Panama seaway through
104 Cenozoic time would have exerted a major influence on the inter-basin carbon reservoir and
105 in setting the modern dissolved inorganic carbon gradients between basins [*Fyke et al.*, 2015].
106 *Pagani et al.* [2011] utilize an Eocene UVic simulation to generate Eocene-Oligocene surface
107 ocean phosphate concentrations, which they further use to compute surface ocean CO₂
108 concentrations to ultimately constrain their reconstructions of atmospheric CO₂ across the
109 EOT. Their results also suggest that, compared to modern, the surface ocean phosphate
110 concentration increases in the low latitudes and decreases in the high latitudes.

111 Here, we revisit the question of the biogeochemical impacts of DP using a more
112 sophisticated, fully coupled, IPCC-class model with, for the first time, a focus on
113 paleoproductivity changes and we compare our results with long-term records of productivity
114 change from the late Eocene to Oligocene. It should be noted that *Winguth et al.* [2012] also
115 applied a fully-coupled IPCC-class GCM to investigate paleoproductivity changes during the
116 Eocene, but their focus was the PETM and as such they realized simulations at different CO₂
117 rather than with open or closed gateways. Assessing the role DP opening played in driving
118 paleoproductivity changes during the late Eocene and Oligocene is important because of its
119 influence on the global carbon cycle and in particular pCO₂ variations, via changes in the
120 oceanic biological pump (see *Hain et al.* [2014] for a review). In the following, we explore
121 the effects of opening DP on long-term productivity changes using a similar approach to that
122 of *Fyke et al.* [2015] and *Elsworth et al.* [2017] in that we employ continental and
123 bathymetric configurations altered from those of present-day. In this respect, strictly speaking,
124 our experiment is a paleogeography sensitivity simulation rather than a simulation of Eocene-

125 Oligocene events. Nevertheless, our approach allows us to isolate the effect of DP opening on
126 global climate and productivity and to make a semi-quantitative comparison to proxy records.
127 Here we focus on comparing our results to records spanning the late Eocene and early
128 Oligocene – the canonical interval for which DP opening is invoked as a climate forcing
129 mechanism – but the possibility that a fully developed ACC was only established during the
130 late Miocene [e.g., *Dalziel et al.*, 2013] also lends our results a longer-term Cenozoic
131 relevance.

132

133 **Models**

134 The results presented in this study are obtained with the IPSL-CM5A Earth System
135 Model [*Dufresne et al.*, 2013], which includes both a representation of the physical
136 atmosphere-ocean-land-sea ice interactions and of the global carbon cycle. Its configuration
137 combines the atmospheric model LMDz [*Hourdin et al.*, 2013], the land-surface model
138 ORCHIDEE [*Krinner et al.*, 2005] and the ocean model NEMOv3.2 [*Madec*, 2008]. The
139 OASIS coupler [*Valcke*, 2006] is used to interpolate and exchange variables and synchronize
140 the models [*Dufresne et al.*, 2013]. Only succinct details about the models will be given here
141 because their full description can be found in *Dufresne et al.* [2013] (see also *Kageyama et al.*
142 [2013] for a description of the model used in paleo configurations for the Last Glacial
143 Maximum and the mid-Holocene). LMDz solves the equation of atmospheric motion on a
144 regular longitude-latitude grid using σ -P vertical coordinates. The resolution used in this
145 study is 96x95x39 (lon. x lat. x vert.), corresponding to 3.75° of longitude and 1.875° of
146 latitude, and 39 vertical levels irregularly distributed. ORCHIDEE runs on the same grid as
147 LMDz and contains a land-surface scheme that simulates both the energy and water cycles of
148 soils and vegetation and a routing scheme that routes precipitated water to the ocean. 12 Plant
149 Functional Types (PFT) define the vegetation. Although the vegetation cover is imposed in

150 this version of IPSL-CM5A, the PFT phenology is computed interactively given the
151 atmospheric state simulated by LMDz. The NEMO model comprises an ocean dynamics
152 component (OPA, *Madec* [2008]), a thermodynamic-dynamic sea-ice model (LIM2, *Fichefet*
153 *and Morales Maqueda* [1997]), and an ocean biogeochemistry model (PISCES, *Aumont and*
154 *Bopp* [2006]). NEMO uses a tripolar grid in order to avoid North Pole singularity [*Madec and*
155 *Imbard*, 1996], for both dynamics and physics. It has a nominal latitudinal resolution of 2° ,
156 increasing up to 0.5° at the Equator, and a longitudinal resolution of approximately 2° and 31
157 unequally spaced vertical levels, the thickness of which varies from 10 m near the surface to
158 500 m at the bottom. PISCES includes a simple representation of the marine ecosystem and of
159 the main oceanic biogeochemical cycles [*Aumont and Bopp*, 2006]. It explicitly represents
160 two classes of phytoplankton (nanophytoplankton and diatoms), two classes of zooplankton,
161 five pools of nutrients (phosphate, nitrate, silicic acid, ammonium and iron), two classes of
162 particulate organic carbon (small and large) and semi-labile dissolved organic carbon. It also
163 includes dissolved and particulate inorganic carbon, alkalinity and dissolved oxygen. The
164 main biogeochemical interactions, such as photosynthesis, respiration, grazing, particle
165 aggregation and sinking, and remineralization, dictate the spatio-temporal evolution of each
166 pool with respect to each other. Phytoplankton growth is limited by the aforementioned
167 nutrients and by light availability. Ratios of C:N:P in the organic pools are kept constant
168 following *Takahashi et al.* [1985], whereas Fe:C ratios for both phytoplankton classes and
169 Si:C ratios for diatoms are prognostically simulated as a function of the external concentration
170 of nutrients and light availability [*Aumont and Bopp*, 2006]. The full description of the
171 version of PISCES used in this study can be found in *Aumont and Bopp* [2006]. All these
172 models have been validated and used, either separately or together within the IPSL-CM5A
173 model, over a variety of climates that include pre-Quaternary climates [e.g., *Contoux et al.*,
174 2015; *Tan et al.*, 2017], LGM [e.g., *Mariotti et al.*, 2012; *Kageyama et al.*, 2013],

175 preindustrial [*Le Mézo et al.*, 2017] and present-day and future climates [e.g., *Aumont and*
176 *Bopp*, 2006; *Bopp et al.*, 2013; *Tagliabue et al.*, 2014], including the latest IPCC exercise.

177 In a first step, two simulations are run with the fully coupled IPSL-CM5A model.
178 Both simulations have a preindustrial land-sea mask, from which the geometry of the Panama
179 Seaway has been altered to represent mid-Cenozoic tectonic configurations (in practice, this
180 means replacing continental grid points by oceanic grid points, see Supplementary Fig. 1). In
181 addition, the land-sea mask of the first simulation, named DC (for Drake Closed), has been
182 modified to add terrestrial points at the Drake Passage to simulate its closure. Conversely, the
183 Drake Passage is left unchanged from that of the preindustrial in the land-sea mask of the
184 second simulation, named DO (Drake Opened). Compared to preindustrial conditions, ice
185 sheets over polar continents have been removed and replaced by tundra-like vegetation but
186 otherwise the preindustrial vegetation cover is kept for both simulations. The ocean is
187 initialized as homogeneous in salinity (34.5 kg.m^{-3}) and with surface temperature following a
188 latitudinal profile ranging from 9°C at the poles to 36°C at the equator. The deep ocean is
189 initialized at a uniform temperature of 7°C (Supplementary Fig. 2). There is no sea ice at the
190 beginning of the simulations. We prescribe a CO_2 concentration of 1120 ppm, which is
191 consistent with most of the records of paleo- CO_2 levels for the Eocene [*Berling and Royer*,
192 2011] and justifies the absence of ice sheets over the poles because the inception of ice over
193 Antarctica is thought to occur at lower CO_2 levels [*Gasson et al.*, 2014; *Ladant et al.*, 2014;
194 *Heureux and Rickaby*, 2015]. Each of the two experiments is run for 1000 years. We
195 acknowledge here that longer integrations (≥ 3000 years) are desirable but we are precluded
196 by the computational performances of this version of the IPSL-CM5A model. However, after
197 1000 years, the surface ocean is in equilibrium and the very small residual trend (< 0.1
198 $^{\circ}\text{C}/\text{century}$) that exists in the deep ocean is unlikely to significantly affect the outcomes of the
199 study.

200 Oceanic biogeochemical equilibrium typically requires longer simulations to be
201 attained than the dynamical equilibrium [Séférian *et al.*, 2016]. In a second step, we run
202 offline simulations of the PISCES model in order to be closer to the biogeochemical
203 equilibrium. PISCES is initialized with the oceanic biogeochemical outputs from the last year
204 of DC and DO coupled experiments and forced by the ocean dynamical fields of DC and DO.
205 In detail, the last 100 years of ocean dynamics outputs are passed to PISCES-offline in a
206 repetitive sequence (that is, after each 100 years of simulation, the ocean forcing is repeated
207 for the next 100 years). The simulations DC-P (for DC-PISCES) and DO-P are run for 2000
208 years to ensure equilibrium of the biogeochemical fields. One caveat must be noted here. In
209 this version of IPSL-CM5A, the nutrient delivery to the ocean is fixed. This is an important
210 simplification because under different climates the global amount of nutrients as well as the
211 spatial distribution of nutrient inputs to the ocean (i.e., the intensity and location of the river
212 flows) will be altered. However, as our purpose is to isolate the climatic and biogeochemical
213 effects of DP opening only and to provide insights into its long-term signature in the proxy
214 record, we have kept present-day nutrient inputs in the simulations.

215 In the following, we refer to the closed (open) Drake Passage simulations by DC (DO)
216 regardless of whether we consider the fully coupled IPSLCM5A or the PISCES-offline
217 simulation, but dynamical results utilize the IPSLCM5A simulations while the
218 biogeochemistry is discussed using the PISCES-offline simulations.

219

220 **Results**

221 In the simulations, the opening of DP significantly alters paleoproductivity (i.e., paleo
222 export production). Figure 1 shows the DC and DO global annual export production of
223 organic carbon at 100 m, a commonly used measure of the carbon export into the deep ocean.
224 The major areas contributing to this export are similar in the two simulations (Fig. 1) but in

225 regions such as the low latitude Indian and Pacific oceans, productivity uniformly decreases
226 with DP opening (Figs. 1 and 2). In contrast, in the Southern Ocean, while productivity
227 decreases in the Atlantic sector, it increases in the Pacific and Indian sectors when DP opens.
228 In the zonal average, opening DP yields an increase in carbon export to the deep ocean in the
229 southern high latitudes but a decrease in the low latitudes and northern high latitudes. This
230 dipole pattern of increase in the southern high latitudes and decrease in the low latitudes
231 agrees with the meridional contrast seen in the data (Table 1). The spatial pattern of
232 increase/decrease in our simulations also compares favourably with observations from various
233 drilling locations (Fig. 1).

234 The observed patterns of paleoproductivity change are the consequence of alterations
235 in ocean circulation, which controls the supply of nutrients, essentially nitrate and phosphate,
236 brought from the deep or sub-surface ocean to the surface. The zonally averaged
237 redistribution of nutrients follows a dipole pattern on the vertical (Fig. 3) with a decrease in
238 the intermediate and upper ocean and an increase at depth when DP opens, except in the
239 highest latitudes of the Southern Ocean ($> 60^{\circ}\text{S}$). Indeed, in this region, an increase in the
240 concentration of nutrients occurs throughout the whole water column when DP opens.
241 Vertical gradients in the upper 500 m confirm the decreased nutrient availability in the low
242 latitudes of each basin in DC and the increase in the southern high latitudes (Fig. 4), except in
243 the upper 100 m of the Atlantic sector.

244 The redistribution of nutrients in our simulations directly follows the reorganization of
245 the oceanic thermohaline circulation (Figs. 5 and 6). In DC, the circulation is dominated by a
246 vigorous Southern Hemisphere overturning cell of up to 30 Sv (Fig. 5), which is fed via deep
247 convection (> 2000 m) in the Pacific and Atlantic sectors of the Southern Ocean (Fig. 6).
248 These deep waters then fill the deep ocean globally, circulate northward in the abyss, are
249 strongly upwelled in the low latitudes at depth and return southward between 500 m and 1500

250 m depth. There is no deep-water formation in the Northern Hemisphere and the closed DP
251 prevents the existence of a well-developed ACC. A wind-driven circumpolar circulation still
252 develops around Antarctica under the influence of the Westerlies (Supplementary Fig. 3),
253 which generates upwelling cells carrying waters from the southward branch of the overturning
254 circulation to the surface. Some of these waters then feed the abyssal circulation through deep
255 convection around Antarctica while the remaining fraction is advected northward to feed
256 intermediate and modal ocean circulation [Toggweiler and Samuels, 1993]. The absence of a
257 well-developed ACC leads to enhanced export of warm and salty subtropical waters into the
258 Southern Ocean, increasing the intensity of deep water formation there as well as the
259 southward ocean heat transport [Sijp and England, 2004].

260 Opening DP strongly modifies the global ocean circulation (Fig. 5). Arguably, the
261 major difference lies in the appearance of a vigorous modern-like ACC (Supplementary Fig.
262 3), which interconnects the three major basins from top to bottom and generates a relatively
263 deep Deacon Cell (~ 2000 m), which reflects the existence of deep upwelling cells. The latter
264 are deeper and more expanded towards Antarctica relative to DC, as shown by the overlain
265 isopycnals on Figs. 3a and 3b, and then feed the abyssal and the intermediate/modal
266 circulations as in DC. Abyssal waters formed around Antarctica remain however mostly
267 confined below 2000 m (Fig. 5). The existence of a well-developed ACC limits the advection
268 of warm and salty subtropical waters to the Southern Ocean, which reduces the intensity of
269 deep convection (Fig. 6) because at high latitudes, salinity exerts the dominant control over
270 the stratification of ocean waters [Ferreira *et al.*, 2010; Yang *et al.*, 2014]. A very weak
271 overturning cell appears in the Nordic Seas, promoting modest intermediate water formation
272 (up to ~ 700 m, Fig. 6). The rates of global overturning in DO are thus greatly reduced
273 relative to DC, increasing the residence time of water in the deep ocean.

274 The transition from a well-ventilated DC to a more stagnant DO ocean thereby drives
275 accumulation of nutrients at depth and depletion in the intermediate and upper ocean in DO
276 relative to DC because the reduced ventilation acts to ‘de-homogenize’ the ocean (Fig. 3c). In
277 DC, the much stronger abyssal low latitudes upwelling allow nutrients to be more rapidly
278 exported in the vigorous southward branch of the overturning circulation whereas in DO,
279 these nutrient-rich waters are confined below 2000 m, thus increasing the nutrient
280 concentrations below 2000 m and decreasing them above 2000 m in DO relative to DC.

281 In both simulations, nutrient-enriched waters are then carried to the surface by the
282 Southern Ocean upwelling cells (Figs. 3a and 3b) but because of the intensity and shape of the
283 overturning circulation, the upwelled waters contain more nutrients in DC relative to DO.
284 This is why the subsurface nutrient concentrations between 40°S and 60°S decrease in DO.
285 However, because the upwelling cells are deeper and expand slightly southward in DO, the
286 subsurface of the highest latitude oceans (> 60°S) is enriched in nutrients relative to DC (Figs.
287 3c and 4, again except for the upper 100 m in the Atlantic sector).

288 The decrease in subsurface nutrient concentration in the 40°S-60°S area in DO has
289 important consequences for the low latitude nutrient supply. Indeed, the intermediate and
290 modal waters (IMW) formed in this area are then advected to feed low latitude subsurface
291 waters [*Toggweiler and Samuels, 1993; Sarmiento et al., 2004*]. Because the IMW are poorer
292 in nutrients when DP is open, the supply of nutrients to the low latitudes decreases. In
293 addition, the slight increase in the tilt of the isopycnals in DO between 40°S and 50°S
294 indicates that IMW sink deeper than in DC and consequently may contribute to the decrease
295 in nutrient supply to the subsurface low latitudes waters in DO.

296 While low latitude productivity and export changes are well explained by the
297 decreased nutrient availability resulting from the less dynamic DO ocean, additional processes
298 contribute to the modelled changes in productivity in the Southern Ocean. Indeed, convective

299 mixing, associated with deep-water formation in winter and wind-driven circumpolar
300 currents, heavily influences export productivity patterns at these latitudes (Figs. 1 and 6). In
301 the Pacific sector, the DO deep-water convective areas are significantly shallower and
302 narrower but remain deep enough to increase the productivity because the convection affects
303 water masses significantly enhanced in nutrients. Following the onset of the ACC, a large
304 convection zone appears in the southern Indian Ocean around 50°S, which, albeit relatively
305 shallow (up to 500 m), drives a large increase in productivity (Fig. 1). Similarly, the wider
306 convection zone just offshore Antarctica at the longitude of Africa generates productivity
307 increase. Finally, in the Atlantic sector, the opposite occurs. Deep-water convection is
308 completely shut down in DO in the central South Atlantic Ocean, leading to a substantial area
309 of decreased productivity.

310 Because the PISCES model allows the explicit representation of nanophytoplankton
311 and diatoms, we can also assess the role of these different groups in driving the modelled
312 primary productivity changes (Fig. 7 and Supplementary Fig. 4). In the low latitudes, the
313 decrease in primary productivity is essentially driven by a strong decline in
314 nanophytoplankton productivity whereas diatom productivity, even if contributing much less
315 to the total, remains relatively stable (except in the coastal Indian ocean). In contrast, in the
316 mid- and high-latitudes, diatoms are responsible for a large part of primary productivity
317 changes, and even become the main contributor to productivity changes in the highest
318 latitudes (> 60°S). This is consistent with increased nutrient availability in the highest
319 latitudes of the DO simulation due to the onset of the ACC. For instance, in the South Pacific,
320 even if winter convection zones are shallower and narrower, the enhanced nutrient supply
321 favours diatoms over nanophytoplankton.

322

323 **Discussion**

324 1. Comparison to model simulations

325 Numerous studies have investigated the role of DP on global climate, with varying
326 continental configurations [e.g., *Mikolajewicz et al.*, 1993; *Heinze and Crowley*, 1997;
327 *Toggweiler and Bjornsson*, 2000; *Sijp and England*, 2004; 2005; *Zhang et al.*, 2010; *Sijp et*
328 *al.*, 2011; *Yang et al.*, 2014; *England et al.*, 2017]. Of these, the most relevant simulations to
329 our study are those performed with the same continental configuration, in particular with the
330 Panama seaway open [e.g., *Mikolajewicz et al.*, 1993; *Yang et al.*, 2014; *Fyke et al.*, 2015].
331 Our reasoning here is based on the results of *Yang et al.* [2014] who demonstrated that the
332 impacts of DP are strongly dependant upon the configuration of the Panama seaway. Using
333 the CM2Mc model in a modern configuration (thus a closed Panama seaway), they show that
334 the closure of DP leads to an ocean circulation resembling that of modern, with the notable
335 exception of the suppression of the Antarctic Bottom Water cell in the Atlantic Ocean. This
336 result is broadly confirmed by *England et al.* [2017], in which the same experiment with the
337 fully coupled CSIRO Mk3L model demonstrates that the DP closed configuration exhibits
338 similar rates of NADW and AABW relative to modern. On the contrary, with an open
339 Panama seaway in an otherwise modern continental configuration, *Yang et al.* [2014] show
340 that the closure of DP generates a large and wide Southern overturning cell and suppresses
341 northern sinking. Our results, obtained with an open Panama seaway, are in agreement with
342 the findings of *Yang et al.* [2014], but also with those of *Fyke et al.* [2015] and *Mikolajewicz*
343 *et al.* [1993] who find a similar ocean circulation with a closed Drake – open Panama
344 configuration, albeit with simpler models (EMIC or ocean-only models).

345 Ocean circulation in the presence of an open DP and an open Panama seaway (i.e., the
346 impact of the opening of Panama) has also received considerable attention [e.g., *Mikolajewicz*
347 *et al.*, 1993; *Lunt et al.*, 2008; *Sepulchre et al.*, 2014; *Yang et al.*, 2014; *Fyke et al.*, 2015]. All
348 models ventilate the deep ocean from the South, although with reduced intensity than with a

349 closed DP, whereas the rates of deep-water formation in the North vary greatly between
350 studies. *Yang et al.* [2014] find virtually no difference between a DO configuration with or
351 without an open Panama seaway, that is, in both cases a strong NH deep overturning cell. In
352 their simulations with the UVic model, *Fyke et al.* [2015] obtain a significant reduction in
353 rates of NH deep water formation with an open Panama Gateway, albeit not a shutdown. A
354 similar result is obtained by *Sepulchre et al.* [2014] with the IPSL-CM4 model and by *Lunt et*
355 *al.* [2008] with the HadCM3 model. On the contrary, *Mikolajewicz et al.* [1993] find, with the
356 ocean-only Hamburg model, that a Drake open and Panama open configuration leads to the
357 cessation of the formation of NADW. In our runs, the thermohaline circulation induced by the
358 DO configuration shows a weak NH intermediate water formation, which is close to the no-
359 NADW state of *Mikolajewicz et al.* [1993]. It is interesting to note that the existence and
360 vigour of the NADW rates in these different models might, at least in part, be driven by the
361 geometry and size of the Panama gateway. Indeed, when Panama is closed (i.e. the modern
362 state), all models show NADW formation. Models run with an open but narrow Panama
363 seaway show reduced rates of NADW formation [*Lunt et al.*, 2008; *Sepulchre et al.*, 2014;
364 *Fyke et al.*, 2015] and those run with a wide Panama seaway show NADW shutdown
365 [*Mikolajewicz et al.*, 1993; this study]. Support for this finding comes from the simulations of
366 *Sijp et al.* [2009] and *Sijp et al.* [2011]. In the first of these studies, open and closed DP
367 simulations are performed in a modern continental configuration, that is, with a closed
368 Panama seaway. Their DP open simulations yield significant NADW formation. In the second
369 of these studies, coupled opening of DP and the Tasman gateway is simulated with the
370 Eocene configuration of *Huber et al.* [2003], which features a wide Panama seaway.
371 Interestingly, no NADW forms in these simulations. The simulations of *Yang et al.* [2014]
372 yield contrasting results, however, because, with DP open, vigorous NADW rates exist
373 regardless of whether a wide or a closed Panama seaway is prescribed. We tentatively infer

374 that the different boundary conditions (pCO₂ and ice sheets cover for instance) applied by
375 *Yang et al.* [2014] and in our study may play a role. In particular, the effect of pCO₂ on ocean
376 circulation may explain part of the discrepancy between the strong NADW rates found in the
377 fully coupled GCM used by *Yang et al.* [2014] and our weak intermediate water formation
378 state (see discussions in *Lunt et al.* [2010], *Donnadieu et al.* [2016] and *Winguth et al.*
379 [2012]). In this regard, it is also interesting to note that the no-NADW simulations of *Sijp et*
380 *al.* [2011] are run, as in our study, with elevated pCO₂. Another factor that should not be
381 ignored is that our fully coupled 1000 year GCM simulations can only be considered to have
382 reached quasi-equilibrium and may miss further reorganizations of ocean circulation.
383 However, although the Northern Hemisphere thermohaline state of the ocean differs between
384 studies, we note that the dynamical results produced by our simulations are consistent with
385 previous findings in that the opening of DP isolates Antarctica from warm and salty
386 subtropical waters, which acts to freshen and cool most of the surface Southern Ocean
387 (Supplementary Fig. 5). We conclude this climatic comparison by acknowledging that many
388 important studies involving the opening of DP (or Tasman gateway) have been carried out
389 using Eocene boundary conditions [e.g., *Huber et al.*, 2003; *Huber et al.*, 2004; *Huber and*
390 *Nof*, 2006; *Zhang et al.*, 2010; *Sijp et al.*, 2011] but the idealized character of our modelling
391 setup makes a direct comparison with these studies more questionable.

392 Two previous numerical studies are particularly relevant to our findings because they
393 numerically address the impact of gateways opening on the biogeochemical state of the ocean,
394 using the spatially resolved, albeit simpler, UVic climate-biogeochemical model [*Pagani et*
395 *al.*, 2011; *Fyke et al.*, 2015]. In line with the findings of *Fyke et al.* [2015] (their figure 9),
396 opening DP in our simulations increases DIC concentrations at depth in all basins although
397 we do not observe a shift from a higher Atlantic DIC concentration to a higher Pacific DIC
398 concentration (not shown). Our results also broadly agree with those of *Pagani et al.* [2011]

399 who show that the surface phosphate concentration in their Eocene simulation features a
400 spatially uniform increase in the low latitudes and decrease in the southern high latitudes
401 relative to modern, attributed to the shallower Eocene Southern Ocean upwelling cells relative
402 to modern induced by the gateways configurations. However, in our experiments, the changes
403 in surface nutrient concentrations in the southern high-latitudes are heterogeneous with areas
404 of increase and decrease. Because we can unambiguously attribute the reorganization of
405 surface nutrient concentration to DP opening in our simulations, we speculate that the
406 gateways impact in the work of *Pagani et al.* [2011] is intertwined with other drivers, such as
407 the much higher CO₂ concentration and other geographical characteristics imposed in their
408 Eocene run relative to their modern.

409

410 2. Comparison to observations

411 Many data studies have investigated paleoproductivity changes during the Eocene and
412 Oligocene [e.g., *Siesser, 1995; Diester-Haass and Zahn, 1996; Salamy and Zachos, 1999;*
413 *Diester-Haass and Zahn, 2001; Diester-Haass and Zachos, 2003; Nilsen et al., 2003;*
414 *Schumacher and Lazarus, 2004; Dunkley Jones et al., 2008; Griffith et al., 2010; Coxall and*
415 *Wilson, 2011; Egan et al., 2013; Moore et al., 2014; Planq et al., 2014; Villa et al., 2014]*
416 but the imprint of tectonics, particularly DP opening, is complex to decipher unambiguously
417 because other climatic shifts, such as the EOT glaciation, occur contemporaneously.
418 However, by investigating exclusively the effects of DP opening in a warmer world, our
419 simulations provide insights on this possible imprint. It is particularly interesting to note that,
420 when compared to records that span an interval longer than the EOT glaciation event, model
421 results are qualitatively consistent with data (Fig. 1), suggesting that, if the DP was
422 sufficiently well breached by the early Oligocene, at least part of the long-term
423 paleoproductivity signal recorded in the data may be attributed to its opening. Our results

424 suggest that DP opening drove a significant reduction in paleoproductivity in the low latitude
425 oceans – a finding consistent with long-term recorded changes, especially in the Eastern
426 Equatorial Pacific [*Schumacher and Lazarus, 2004; Moore et al., 2014*] and in the Equatorial
427 Indian Ocean [*Siesser, 1995*]. In the high latitudes, most long-term records document an
428 increase in paleoproductivity [e.g., *Diester-Haass and Zahn, 1996; 2001; Schumacher and*
429 *Lazarus, 2004*], but the pattern of paleoproductivity increase/decrease simulated by the model
430 is not uniform and strongly related to variations in the convective mixing areas.

431 Our simple model-data comparison is similar to that of *Winguth et al. [2012]*. A more
432 in-depth analysis is unwarranted because we present a paleogeography sensitivity simulation
433 rather than an attempt to simulate Eocene-Oligocene events *sensu stricto*. Furthermore,
434 different data sets produce sometimes contrasting indications of paleoproductivity change
435 even when taken from the same site. A good example comes in the paleoproductivity records
436 from the Eastern Equatorial Pacific [e.g., *Coxall and Wilson, 2011; Erhardt et al., 2013;*
437 *Moore et al., 2014*]. Although there are reasonable explanations to these discrepancies
438 [*Erhardt et al., 2013; Moore et al., 2014*], this observation highlights the complexity
439 associated with reconstructing paleoproductivity from proxy signals [*Anderson and Delaney,*
440 *2005*]. In the high latitudes, many records show significant enhancement of the
441 paleoproductivity during the EOT event [e.g., *Salamy and Zachos, 1999; Diester-Haass and*
442 *Zahn, 2001; Planq et al., 2014; Villa et al., 2014*] or during the latest Eocene [*Diekmann et*
443 *al., 2004; Egan et al., 2013; Villa et al., 2014*]. In particular, during the latter, it has been
444 argued that pulses of tectonic opening of DP [*Scher and Martin, 2006*] may play a role in the
445 transition from oligotrophic to eutrophic nannofossils taxa [*Villa et al., 2014*] or an increase
446 in diatom abundance [*Egan et al., 2013*]. Based on Si isotopes records, *Egan et al. [2013]*
447 invoke increased diatom primary productivity to explain the recorded increased silicic acid
448 utilization at the surface at Site 1090. Although our modelled results support a net decrease in

449 diatoms (and nanophytoplankton) primary production in most of the South Atlantic Ocean
450 (Fig. 7), the simulated export production increases at Sites 689 [Villa *et al.*, 2014] and 1090
451 [Egan *et al.*, 2013]. Primary and export productivity do indeed not necessarily co-vary as
452 organic matter remineralization, among others, is a function of temperature [John *et al.*,
453 2013]. The significant modelled surface cooling when DP opens at Sites 689 and 1090
454 (Supplementary Fig. 5) generates reduced recycling of organic matter and may thus explain
455 the contrasting variations of primary and export productivity.

456

457 3. Caveats related to the idealized framework of the study

458 Taken at face value, our simulated paleoproductivity changes fit marine records
459 reasonably well, but important caveats must be kept in mind when interpreting our model
460 results. First, we do not use a realistic late Eocene global paleogeography, either regarding the
461 geometry of important gateways or other major tectonic differences such as the existence of
462 the Tethys Sea or the position and height of the Tibetan Plateau. Our idealized simulations
463 therefore remain a sensitivity experiment to the opening of DP. Because our simulated
464 paleoproductivity changes are essentially driven by the onset of the ACC, the impact of a
465 closed or restricted Tasman seaway prior to the latest Eocene [Huber *et al.*, 2004; Stickley *et*
466 *al.*, 2004] may have important consequences for paleoproductivity patterns. However, a
467 recent idealized study suggests that a circumpolar water path, which would circumvent
468 Australia, could exist even in the absence of an open Tasman seaway [Munday *et al.*, 2015].
469 Second, our simulations were performed using two end-member boundary conditions (DP
470 closed and DP open) that are not strictly representative of the late Eocene and Oligocene, as
471 some evidence points to initial opening of DP as early as the Early Eocene [Eagles *et al.*,
472 2006; Eagles and Jokat, 2014]. The climatic relevance of an incipient opening is intuitively
473 questionable and the concept of a threshold relationship between gateway opening and

474 climate response is appealing. *Sijp and England* [2005] argued that the sill depth of DP
475 critically impacted the global ocean circulation, because it was instrumental in controlling the
476 formation of NADW, but this result was obtained with a closed Panama Seaway, which is a
477 configuration that favours NADW formation [*Lunt et al.*, 2008; *Sepulchre et al.*, 2014; *Yang*
478 *et al.*, 2014]. The open Panama simulations performed here are not sufficient to
479 unambiguously answer this question. Finally, our offline PISCES simulations are run with
480 fixed nutrient supply from rivers, which are unaffected by variations in runoff whereas we
481 know that changes in nutrient and carbonate supply down rivers across the Eocene Oligocene
482 Transition are both likely and capable of driving major change in global carbon cycling
483 [*Coxall et al.*, 2005; *Dunkley Jones et al.*, 2008; *Merico et al.*, 2008; *Armstrong McKay et al.*,
484 2016].

485

486 **Conclusion**

487 Using the IPSL-CM5A coupled model we have shown that the opening of Drake
488 Passage profoundly alters oceanic paleoproductivity patterns across the globe. The
489 reorganization of the oceanic circulation, from a well-ventilated ocean when Drake Passage is
490 closed to a more stagnant state when Drake Passage is open, drives subsurface nutrient
491 depletion in the low latitudes. Nanophytoplankton, rather than diatoms – possibly because the
492 latter are only marginal contributors to the modelled low latitude primary productivity, are
493 strongly affected by this depletion and the productivity consequently declines, especially in
494 the Pacific and Indian oceans. In the high latitudes, productivity changes are driven both by
495 nutrient availability and areas of convective mixing, which generate zones of productivity
496 increase (most of the southern Pacific and Indian oceans) and decrease (most of the South
497 Atlantic Ocean). In contrast to the low latitudes, diatoms are largely responsible for these
498 productivity variations, especially in the southernmost latitudes. A simple qualitative

499 comparison with geological records reveals a good match between locations of
500 paleoproductivity changes simulated by the model and inferred from data, suggesting that the
501 role of Drake Passage opening in driving part of the long-term productivity signal across the
502 late Eocene and early Oligocene may be non-negligible.

503

504

505

506

507

508

509

510

511

512

513

514

515

516

517

518

519

520

521

522

523

524 **Acknowledgements**

525 We are grateful to J.R. Toggweiler, Willem Sijp and Matt Huber for their insightful
526 comments, and to Ellen Thomas for editorial handling. We thank the CEA/CCRT for
527 providing access to the HPC resources of TGCC under the allocation 2014-012212 made by
528 GENCI. We acknowledge the support of the project Anox-Sea funded by the ANR under the
529 grant number ANR-12-BS06-0011-03. Long-term storage of the initial and boundary
530 conditions and of the key climatological and biogeochemical outputs of the simulations will
531 be performed at the LSCE storage system and/or at the TGCC storage system. We
532 acknowledge use of the Panoply (www.giss.nasa.gov/tools/panoply/) and Ferret
533 (ferret.pmel.noaa.gov/Ferret/) programs for analysis and graphics in this paper.

534

535 **Author Contributions**

536 J.-B.L. designed and performed the numerical simulations, with contributions from Y.D., and
537 wrote the draft of the manuscript. All authors analysed and discussed the results and
538 contributed to the final version of the manuscript.

539

540 **Additional Information**

541 The authors declare no competing financial interest. Correspondence and requests for
542 materials should be addressed to either J.-B.L. (jbladant@gmail.com) or Y.D.
543 (donnadieu@cerege.fr).

544

545

546

547

548

549 **References**

- 550 Anderson, L. D., and M. L. Delaney (2005), Middle Eocene to early Oligocene
551 paleoceanography from Agulhas Ridge, Southern Ocean (Ocean Drilling Program Leg
552 177, Site 1090), *Paleoceanography*, 20(1).
- 553 Armstrong McKay, D. I., T. Tyrrell, and P. A. Wilson (2016), Global carbon cycle
554 perturbation across the Eocene - Oligocene climate transition, *Paleoceanography*.
- 555 Aumont, O., and L. Bopp (2006), Globalizing results from ocean in situ iron fertilization
556 studies, *Global Biogeochemical Cycles*, 20(2).
- 557 Barker, P., and J. Burrell (1977), The opening of Drake passage, *Marine geology*, 25(1),
558 15-34.
- 559 Barker, P. F., G. M. Filippelli, F. Florindo, E. E. Martin, and H. D. Scher (2007), Onset and
560 role of the Antarctic Circumpolar Current, *Deep Sea Research Part II: Topical Studies in*
561 *Oceanography*, 54(21), 2388-2398.
- 562 Beerling, D. J., and D. L. Royer (2011), Convergent Cenozoic CO₂ history, *Nature*
563 *Geoscience*, 4(7), 418-420.
- 564 Bopp, L., L. Resplandy, J. C. Orr, S. C. Doney, J. P. Dunne, M. Gehlen, P. Halloran, C. Heinze,
565 T. Ilyina, and R. Seferian (2013), Multiple stressors of ocean ecosystems in the 21st
566 century: projections with CMIP5 models, *Biogeosciences*, 10, 6225-6245.
- 567 Contoux, C., C. Dumas, G. Ramstein, A. Jost, and A. M. Dolan (2015), Modelling Greenland
568 ice sheet inception and sustainability during the Late Pliocene, *Earth and Planetary*
569 *Science Letters*, 424, 295-305.
- 570 Coxall, H. K., and P. A. Wilson (2011), Early Oligocene glaciation and productivity in the
571 eastern equatorial Pacific: Insights into global carbon cycling, *Paleoceanography*, 26(2).
- 572 Coxall, H. K., P. A. Wilson, H. Pälike, C. H. Lear, and J. Backman (2005), Rapid stepwise
573 onset of Antarctic glaciation and deeper calcite compensation in the Pacific Ocean,
574 *Nature*, 433(7021), 53-57.
- 575 Dalziel, I. W. D., L. A. Lawver, J. A. Pearce, P. F. Barker, A. R. Hastie, D. N. Barfod, H. W.
576 Schenke, and M. B. Davis (2013), A potential barrier to deep Antarctic circumpolar flow
577 until the late Miocene?, *Geology*, 41(9), 947-950.
- 578 DeConto, R. M., and D. Pollard (2003), Rapid Cenozoic glaciation of Antarctica induced by
579 declining atmospheric CO₂, *Nature*, 421, 245-249.
- 580 Diekmann, B., G. Kuhn, R. Gersonde, and A. Mackensen (2004), Middle Eocene to early
581 Miocene environmental changes in the sub-Antarctic Southern Ocean: evidence from
582 biogenic and terrigenous depositional patterns at ODP Site 1090, *Global and Planetary*
583 *Change*, 40(3), 295-313.
- 584 Diester-Haass, L., and R. Zahn (1996), Eocene-Oligocene transition in the Southern
585 Ocean: History of water mass circulation and biological productivity, *Geology*, 24(2),
586 163-166.
- 587 Diester-Haass, L., and R. Zahn (2001), Paleoproductivity increase at the
588 Eocene-Oligocene climatic transition: ODP/DSDP Sites 763 and 592, *Palaeogeography,*
589 *Palaeoclimatology, Palaeoecology*, 172(1), 153-170.
- 590 Diester-Haass, L., and J. Zachos (2003), The Eocene-Oligocene transition in the
591 Equatorial Atlantic (ODP Site 925); paleoproductivity increase and positive δ¹³C
592 excursion., in *From greenhouse to icehouse; the marine Eocene-Oligocene transition,*
593 edited by D. R. Prothero, L. C. Ivany and E. A. Nesbitt, Columbia University Press, New
594 York, NY, USA.

595 Donnadieu, Y., E. Puc at, M. Moiroud, F. Guillocheau, and J.-F. Deconinck (2016), A
596 better-ventilated ocean triggered by Late Cretaceous changes in continental
597 configuration, *Nature communications*, 7.

598 Dufresne, J. L., et al. (2013), Climate change projections using the IPSL-CM5 Earth
599 System Model: from CMIP3 to CMIP5, *Climate Dynamics*, 40(9-10), 2123-2165.

600 Dunkley Jones, T., P. R. Bown, P. N. Pearson, B. S. Wade, H. K. Coxall, and C. H. Lear
601 (2008), Major shifts in calcareous phytoplankton assemblages through the Eocene -
602 Oligocene transition of Tanzania and their implications for low - latitude primary
603 production, *Paleoceanography*, 23(4).

604 Eagles, G., and W. Jokat (2014), Tectonic reconstructions for paleobathymetry in Drake
605 Passage, *Tectonophysics*, 611, 28-50.

606 Eagles, G., R. Livermore, and P. Morris (2006), Small basins in the Scotia Sea: the Eocene
607 Drake passage gateway, *Earth and Planetary Science Letters*, 242(3), 343-353.

608 Egan, K. E., R. E. M. Rickaby, K. R. Hendry, and A. N. Halliday (2013), Opening the
609 gateways for diatoms primes Earth for Antarctic glaciation, *Earth and Planetary Science
610 Letters*, 375, 34-43.

611 Elsworth, G., E. Galbraith, G. Halverson, and S. Yang (2017), Enhanced weathering and
612 CO2 drawdown caused by latest Eocene strengthening of the Atlantic meridional
613 overturning circulation, *Nature Geoscience*, 10(3), 213-216.

614 England, M. H., D. K. Hutchinson, A. Santoso, and W. P. Sijp (2017), Ice-atmosphere
615 feedbacks dominate the response of the climate system to Drake Passage closure,
616 *Journal of Climate*(2017).

617 Erhardt, A. M., H. P alike, and A. Paytan (2013), High - resolution record of export
618 production in the eastern equatorial Pacific across the Eocene - Oligocene transition
619 and relationships to global climatic records, *Paleoceanography*, 28(1), 130-142.

620 Faul, K. L., and M. L. Delaney (2010), A comparison of early Paleogene export
621 productivity and organic carbon burial flux for Maud Rise, Weddell Sea, and Kerguelen
622 Plateau, south Indian Ocean, *Paleoceanography*, 25(3).

623 Ferreira, D., J. Marshall, and J.-M. Campin (2010), Localization of deep water formation:
624 Role of atmospheric moisture transport and geometrical constraints on ocean
625 circulation, *Journal of Climate*, 23(6), 1456-1476.

626 Fichfet, T., and M. A. Morales Maqueda (1997), Sensitivity of a global sea ice model to
627 the treatment of ice thermodynamics and dynamics, *Journal of Geophysical Research:
628 Oceans (1978-2012)*, 102(C6), 12609-12646.

629 Fyke, J. G., M. D'Orgeville, and A. J. Weaver (2015), Drake Passage and Central American
630 Seaway controls on the distribution of the oceanic carbon reservoir, *Global and
631 Planetary Change*, 128, 72-82.

632 Gasson, E., et al. (2014), Uncertainties in the modelled CO2 threshold for Antarctic
633 glaciation, *Climate of the Past*, 10(2), 451-466.

634 Goldner, A., N. Herold, and M. Huber (2014), Antarctic glaciation caused ocean
635 circulation changes at the Eocene-Oligocene transition, *Nature*, 511(7511), 574-577.

636 Griffith, E., M. Calhoun, E. Thomas, K. Averyt, A. Erhardt, T. Bralower, M. Lyle, A.
637 Olivarez - Lyle, and A. Paytan (2010), Export productivity and carbonate accumulation
638 in the Pacific Basin at the transition from a greenhouse to icehouse climate (late Eocene
639 to early Oligocene), *Paleoceanography*, 25(3).

640 Hain, M. P., D. M. Sigman, and G. H. Haug (2014), 8.18 The Biological Pump in the Past,
641 *Reference Module in Earth Systems and Environmental Sciences, Treatise on Geochemistry*,
642 485-517.

643 Heinze, C., and T. J. Crowley (1997), Sedimentary response to ocean gateway circulation
644 changes, *Paleoceanography*, 12(6), 742-754.

645 Heuroux, A. M. C., and R. E. M. Rickaby (2015), Refining our estimate of atmospheric CO₂
646 across the Eocene–Oligocene climatic transition, *Earth and Planetary Science Letters*,
647 409, 329-338.

648 Hourdin, F., M.-A. Foujols, F. Codron, V. Guemas, J.-L. Dufresne, S. Bony, S. Denvil, L. Guez,
649 F. Lott, and J. Ghattas (2013), Impact of the LMDZ atmospheric grid configuration on the
650 climate and sensitivity of the IPSL-CM5A coupled model, *Climate Dynamics*, 40(9-10),
651 2167-2192.

652 Huber, M., and D. Nof (2006), The ocean circulation in the southern hemisphere and its
653 climatic impacts in the Eocene, *Palaeogeography, Palaeoclimatology, Palaeoecology*,
654 231(1), 9-28.

655 Huber, M., L. C. Sloan, and C. Shellito (2003), Early Paleogene oceans and climate: A fully
656 coupled modeling approach using the NCAR CCSM, *Geological Society of America Special
657 Papers*, 369, 25-47.

658 Huber, M., H. Brinkhuis, C. E. Stickley, K. Döös, A. Sluijs, J. Warnaar, S. A. Schellenberg,
659 and G. L. Williams (2004), Eocene circulation of the Southern Ocean: Was Antarctica
660 kept warm by subtropical waters?, *Paleoceanography*, 19(4), PA4026.

661 John, E. H., P. N. Pearson, H. K. Coxall, H. Birch, B. S. Wade, and G. L. Foster (2013), Warm
662 ocean processes and carbon cycling in the Eocene, *Phil. Trans. R. Soc. A*, 371(2001),
663 20130099.

664 Kageyama, M., et al. (2013), Mid-Holocene and Last Glacial Maximum climate
665 simulations with the IPSL model—part I: comparing IPSL_CM5A to IPSL_CM4, *Climate
666 Dynamics*, 40(9-10), 2447-2468.

667 Katz, M. E., B. S. Cramer, J. R. Toggweiler, G. Esmay, C. Liu, K. G. Miller, Y. Rosenthal, B. S.
668 Wade, and J. D. Wright (2011), Impact of Antarctic Circumpolar Current Development on
669 Late Paleogene Ocean Structure, *Science*, 332(6033), 1076-1079.

670 Kennett, J. P. (1977), Cenozoic evolution of Antarctic glaciation, the circum-Antarctic
671 Ocean, and their impact on global paleoceanography, *Journal of Geophysical Research*,
672 82(27), 3843-3860.

673 Krinner, G., N. Viovy, N. de Noblet - Ducoudré, J. Ogée, J. Polcher, P. Friedlingstein, P.
674 Ciais, S. Sitch, and I. C. Prentice (2005), A dynamic global vegetation model for studies of
675 the coupled atmosphere - biosphere system, *Global Biogeochemical Cycles*, 19(1).

676 Ladant, J.-B., Y. Donnadieu, V. Lefebvre, and C. Dumas (2014), The respective role of
677 atmospheric carbon dioxide and orbital parameters on ice sheet evolution at the
678 Eocene-Oligocene transition, *Paleoceanography*, 29(8), 810-823.

679 Lagabrielle, Y., Y. Goddérès, Y. Donnadieu, J. Malavieille, and M. Suarez (2009), The
680 tectonic history of Drake Passage and its possible impacts on global climate, *Earth and
681 Planetary Science Letters*, 279(3-4), 197-211.

682 Le Mézo, P., L. Beaufort, L. Bopp, P. Braconnot, and M. Kageyama (2017), From monsoon
683 to marine productivity in the Arabian Sea: insights from glacial and interglacial climates,
684 *Climate of the Past*, 13(7), 759-778.

685 Lear, C. H., and D. J. Lunt (2016), How Antarctica got its ice, *Science*, 352(6281), 34-35.

686 Lear, C. H., H. Elderfield, and P. A. Wilson (2000), Cenozoic deep-sea temperatures and
687 global ice volumes from Mg/Ca in benthic foraminiferal calcite, *Science*, 287(5451), 269-
688 272.

689 Lunt, D. J., P. J. Valdes, A. Haywood, and I. C. Rutt (2008), Closure of the Panama Seaway
690 during the Pliocene: implications for climate and Northern Hemisphere glaciation,
691 *Climate Dynamics*, 30(1), 1-18.

692 Lunt, D. J., P. J. Valdes, T. D. Jones, A. Ridgwell, A. M. Haywood, D. N. Schmidt, R. Marsh,
693 and M. Maslin (2010), CO₂-driven ocean circulation changes as an amplifier of
694 Paleocene-Eocene thermal maximum hydrate destabilization, *Geology*, 38(10), 875-878.
695 Madec, G. (2008), NEMO ocean engine. Technical note. *Rep.*, IPSL.
696 Madec, G., and M. Imbard (1996), A global ocean mesh to overcome the North Pole
697 singularity, *Climate Dynamics*, 12(6), 381-388.
698 Mariotti, V., L. Bopp, A. Tagliabue, M. Kageyama, and D. Swingedouw (2012), Marine
699 productivity response to Heinrich events: a model-data comparison, *Climate of the Past*,
700 8(5), 1581.
701 Matthews, R. K., and R. Z. Poore (1980), Tertiary δ 180 record and glacio-eustatic sea-
702 level fluctuations, *Geology*, 8(10), 501-504.
703 Merico, A., T. Tyrrell, and P. A. Wilson (2008), Eocene/Oligocene ocean de-acidification
704 linked to Antarctic glaciation by sea-level fall, *Nature*, 452(7190), 979-982.
705 Mikolajewicz, U., E. Maier-Reimer, T. J. Crowley, and K.-Y. Kim (1993), Effect of Drake
706 and Panamanian gateways on the circulation of an ocean model, *Paleoceanography*, 8(4),
707 409-426.
708 Miller, K. G., J. D. Wright, and R. G. Fairbanks (1991), Unlocking the ice house:
709 Oligocene - Miocene oxygen isotopes, eustasy, and margin erosion, *Journal of*
710 *Geophysical Research: Solid Earth*, 96(B4), 6829-6848.
711 Moore, T. C., B. S. Wade, T. Westerhold, A. M. Erhardt, H. K. Coxall, J. Baldauf, and M.
712 Wagner (2014), Equatorial Pacific productivity changes near the Eocene - Oligocene
713 boundary, *Paleoceanography*, 29(9), 825-844.
714 Munday, D. R., H. L. Johnson, and D. P. Marshall (2015), The role of ocean gateways in the
715 dynamics and sensitivity to wind stress of the early Antarctic Circumpolar Current,
716 *Paleoceanography*, 30(3), 284-302.
717 Nilsen, E. B., L. D. Anderson, and M. L. Delaney (2003), Paleoproductivity, nutrient burial,
718 climate change and the carbon cycle in the western equatorial Atlantic across the
719 Eocene/Oligocene boundary, *Paleoceanography*, 18(3).
720 Pagani, M., M. Huber, Z. Liu, S. M. Bohaty, J. Henderiks, W. Sijp, S. Krishnan, and R. M.
721 DeConto (2011), The Role of Carbon Dioxide During the Onset of Antarctic Glaciation,
722 *Science*, 334(6060), 1261-1264.
723 Pälike, H., et al. (2012), A Cenozoic record of the equatorial Pacific carbonate
724 compensation depth, *Nature*, 488(7413), 609-614.
725 Pearson, P. N., G. L. Foster, and B. S. Wade (2009), Atmospheric carbon dioxide through
726 the Eocene–Oligocene climate transition, *Nature*, 461(7267), 1110-1113.
727 Plancq, J., E. Mattioli, B. Pittet, L. Simon, and V. Grossi (2014), Productivity and sea-
728 surface temperature changes recorded during the late Eocene–early Oligocene at DSDP
729 Site 511 (South Atlantic), *Palaeogeography, Palaeoclimatology, Palaeoecology*, 407, 34-
730 44.
731 Salamy, K. A., and J. C. Zachos (1999), Latest Eocene–Early Oligocene climate change and
732 Southern Ocean fertility: inferences from sediment accumulation and stable isotope
733 data, *Palaeogeography, Palaeoclimatology, Palaeoecology*, 145(1), 61-77.
734 Sarmiento, J. L., N. Gruber, M. A. Brzezinski, and J. P. Dunne (2004), High-latitude
735 controls of thermocline nutrients and low latitude biological productivity, *Nature*,
736 427(6969), 56-60.
737 Scher, H., and E. Martin (2006), Timing and climatic consequences of the opening of
738 Drake Passage, *Science*, 312(5772), 428-430.

739 Scher, H., J. M. Whittaker, S. E. Williams, J. C. Latimer, W. E. Kordesch, and M. L. Delaney
740 (2015), Onset of Antarctic Circumpolar Current 30 million years ago as Tasmanian
741 Gateway aligned with westerlies, *Nature*, 523(7562), 580-583.

742 Schumacher, S., and D. Lazarus (2004), Regional differences in pelagic productivity in
743 the late Eocene to early Oligocene—a comparison of southern high latitudes and lower
744 latitudes, *Palaeogeography, palaeoclimatology, palaeoecology*, 214(3), 243-263.

745 Séférian, R., et al. (2016), Inconsistent strategies to spin up models in CMIP5:
746 implications for ocean biogeochemical model performance assessment, *Geoscientific
747 Model Development*, 9(5), 1827-1851.

748 Sepulchre, P., T. Arsouze, Y. Donnadieu, J. C. Dutay, C. Jaramillo, J. Le Bras, E. Martin, C.
749 Montes, and A. J. Waite (2014), Consequences of shoaling of the Central American
750 Seaway determined from modeling Nd isotopes, *Paleoceanography*, 29(3), 176-189.

751 Siesser, W. G. (1995), Paleoproductivity of the Indian Ocean during the Tertiary period,
752 *Global and Planetary Change*, 11(1-2), 71-88.

753 Sijp, W. P., and M. H. England (2004), Effect of the Drake Passage throughflow on global
754 climate, *Journal of physical oceanography*, 34(5), 1254-1266.

755 Sijp, W. P., and M. H. England (2005), Role of the Drake Passage in controlling the
756 stability of the ocean's thermohaline circulation, *Journal of climate*, 18(12), 1957-1966.

757 Sijp, W. P., M. H. England, and J. R. Toggweiler (2009), Effect of ocean gateway changes
758 under greenhouse warmth, *Journal of Climate*, 22(24), 6639-6652.

759 Sijp, W. P., M. H. England, and M. Huber (2011), Effect of the deepening of the Tasman
760 Gateway on the global ocean, *Paleoceanography*, 26(4), PA4207.

761 Stickley, C. E., H. Brinkhuis, S. A. Schellenberg, A. Sluijs, U. Röhl, M. Fuller, M. Grauert, M.
762 Huber, J. Warnaar, and G. L. Williams (2004), Timing and nature of the deepening of the
763 Tasmanian Gateway, *Paleoceanography*, 19(4), PA4027

764 Tagliabue, A., O. Aumont, and L. Bopp (2014), The impact of different external sources of
765 iron on the global carbon cycle, *Geophysical Research Letters*, 41(3), 920-926.

766 Takahashi, T., W. S. Broecker, and S. Langer (1985), Redfield ratio based on chemical
767 data from isopycnal surfaces, *Journal of Geophysical Research: Oceans*, 90(C4), 6907-
768 6924.

769 Tan, N., G. Ramstein, C. Dumas, C. Contoux, J.-B. Ladant, P. Sepulchre, Z. Zhang, and S. De
770 Schepper (2017), Exploring the MIS M2 glaciation occurring during a warm and high
771 atmospheric CO₂ Pliocene background climate, *Earth and Planetary Science Letters*, 472,
772 266-276.

773 Toggweiler, J., and H. Bjornsson (2000), Drake Passage and palaeoclimate, *Journal of
774 Quaternary Science*, 15(4), 319-328.

775 Toggweiler, J. R., and B. Samuels (1993), New radiocarbon constraints on the upwelling
776 of abyssal water to the ocean's surface., in *The global carbon cycle.*, edited by M.
777 Heimann, pp. 333-366, Springer, Berlin, Heidelberg.

778 Valcke, S. (2006), OASIS user's guide (prism-2.5). Tech. Rep. TR/CMGC/06/73, PRISM
779 Report No3.Rep., CERFACS, Toulouse, France.

780 Villa, G., C. Fioroni, D. Persico, A. P. Roberts, and F. Florindo (2014), Middle Eocene to
781 Late Oligocene Antarctic glaciation/deglaciation and southern ocean productivity,
782 *Paleoceanography*, 29(3), 223-237.

783 Winguth, A. M. E., E. Thomas, and C. Winguth (2012), Global decline in ocean ventilation,
784 oxygenation, and productivity during the Paleocene-Eocene Thermal Maximum:
785 Implications for the benthic extinction, *Geology*, 40(3), 263-266.

786 Yang, S., E. Galbraith, and J. Palter (2014), Coupled climate impacts of the Drake Passage
787 and the Panama Seaway, *Climate Dynamics*, 43(1-2), 37-52.

788 Zachos, J. C., and L. R. Kump (2005), Carbon cycle feedbacks and the initiation of
789 Antarctic glaciation in the earliest Oligocene, *Global and Planetary Change*, 47(1), 51-66.
790 Zhang, Z.-S., Q. Yan, and H.-J. Wang (2010), Has the Drake passage played an essential
791 role in the Cenozoic cooling, *Atmos. Oceanic Sci. Lett.*, 3(5), 288-292.
792

793

794 **Legends and Tables**

795

Site (Reference)	Latitude	Longitude	Qualitative productivity change
1209-1211 (Griffith et al. 2010)	~ 20°N	~ 172°W	decrease
925 (Nilsen et al. 2003) *	~ 4°N	~ 43°W	no change
U1333 (Moore et al. 2014)	~ 3°N	~ 113°W	decrease
1218 and U1334 (Moore et al. 2014)	~ 0-2°N	~ 110°W	decrease
462 (Schumacher and Lazarus 2004)	~ 2°S	~ 178°W	no change
959 (Schumacher and Lazarus 2004)	~ 2°S	~ 13°W	slight decrease or no change
574 (Schumacher and Lazarus 2004)	~ 7°S	~ 117°W	slight decrease or no change
709 (Siesser 1995)	~ 10°S	~ 75°E	decrease
758 (Siesser 1995)	~ 10°S	~ 110°E	no change or no data
757 (Siesser 1995)	~ 30°S	~ 95°E	no change
762 (Siesser 1995)	~ 35°S	~ 115°E	decrease
763 (Diester-Haas and Zahn 2001)	~ 40°S	~ 112°E	increase
1090 (Diekmann et al. 2004)	~ 43°S	~ 9°E	decrease
1090 (Egan et al. 2013)	~ 43°S	~ 9°E	increase
752 (Siesser 1995)	~ 45°S	~ 90°E	no change or no data
511 (Plancq et al. 2014)	~ 52°S	~ 42°W	increase
511 (Schumacher and Lazarus 2004)	~ 55°S	~ 42°W	increase
748 (Siesser 1995)	~ 55°S	~ 70°E	no change or no data
592 (Diester-Haas and Zahn 2001)	~ 55°S	~ 165°E	increase
748 (Schumacher and Lazarus 2004)	~ 56°S	~ 73°E	increase
748 (Villa et al. 2014)	~ 57°S	~ 74°E	increase
738 and 744 (Villa et al. 2014) *	~ 63°S	~ 83°E	increase
689 (Schumacher and Lazarus 2004)	~ 72°S	~ 15°W	increase
689 and 690 (Villa et al. 2014)	~ 72°S	~ 15°W	increase

Table 1. Compilation of long-term productivity changes across the late Eocene and early Oligocene. Longitudes and latitudes are approximate paleolocations of the sites. The asterisk denotes sites where modern location is used. There are a few redundant sites but findings from different studies at these sites are similar.

796

797

798 **Figure 1.** (top) Mean annual export production at 100 m ($\text{gC}\cdot\text{m}^{-2}\cdot\text{yr}^{-1}$) for DC and DO
799 simulations. (bottom) Annual export production at 100 m difference between DO and DC
800 ($\text{gC}\cdot\text{m}^{-2}\cdot\text{yr}^{-1}$). Color-coded circles represent productivity variations from data records (see
801 Table 1): red = increase, blue = decrease, pale shading = weak or uncertain variations, white =
802 no variations or lack of data.
803

804

805 **Figure 2.** Zonally averaged export production at 100 m ($\text{gC}\cdot\text{m}^{-2}\cdot\text{yr}^{-1}$) at the global scale and in
806 each basin for DC (black solid lines) and DO (red dashed lines).
807

808

809 **Figure 3.** (top) Mean annual zonally averaged nitrate concentration ($\mu\text{mol}\cdot\text{L}^{-1}$) for DC and
810 DO with density contours ($0.1 \text{ kg}\cdot\text{m}^{-3}$) overlain. (bottom) Mean annual zonally averaged
811 nitrate concentration difference ($\mu\text{mol}\cdot\text{L}^{-1}$) between DO and DC, with density contours (0.1
812 $\text{kg}\cdot\text{m}^{-3}$) overlain in black for DC and green for DO. Note that $1000 \text{ kg}\cdot\text{m}^{-3}$ is subtracted from
813 density values on the plot.
814

815

816 **Figure 4.** Global, Atlantic, Pacific and Indian upper 500 m nitrate concentration gradients in
817 the low latitudes ($40^{\circ}\text{S} - 40^{\circ}\text{N}$, solid lines) and the southern high latitudes ($90^{\circ}\text{S} - 60^{\circ}\text{S}$,
818 dashed lines) for DC (black) and DO (red).
819

820

821 **Figure 5.** Global meridional overturning streamfunction (Sv , clockwise positive) for DC and
822 DO. Contours 4 Sv , negative dashed.
823

824

825 **Figure 6.** Wintertime deep-water formation in the Southern (top) and Northern (bottom)
826 Hemispheres for DF and DO simulations, as represented by the ocean mixed-layer depth (m).
827 Note that the scale differs between southern and northern plots.
828

829

830 **Figure 7.** Diatoms and nanophytoplankton primary production difference ($\text{gC}\cdot\text{m}^{-2}\cdot\text{yr}^{-1}$)
831 between DO and DC.
832

833

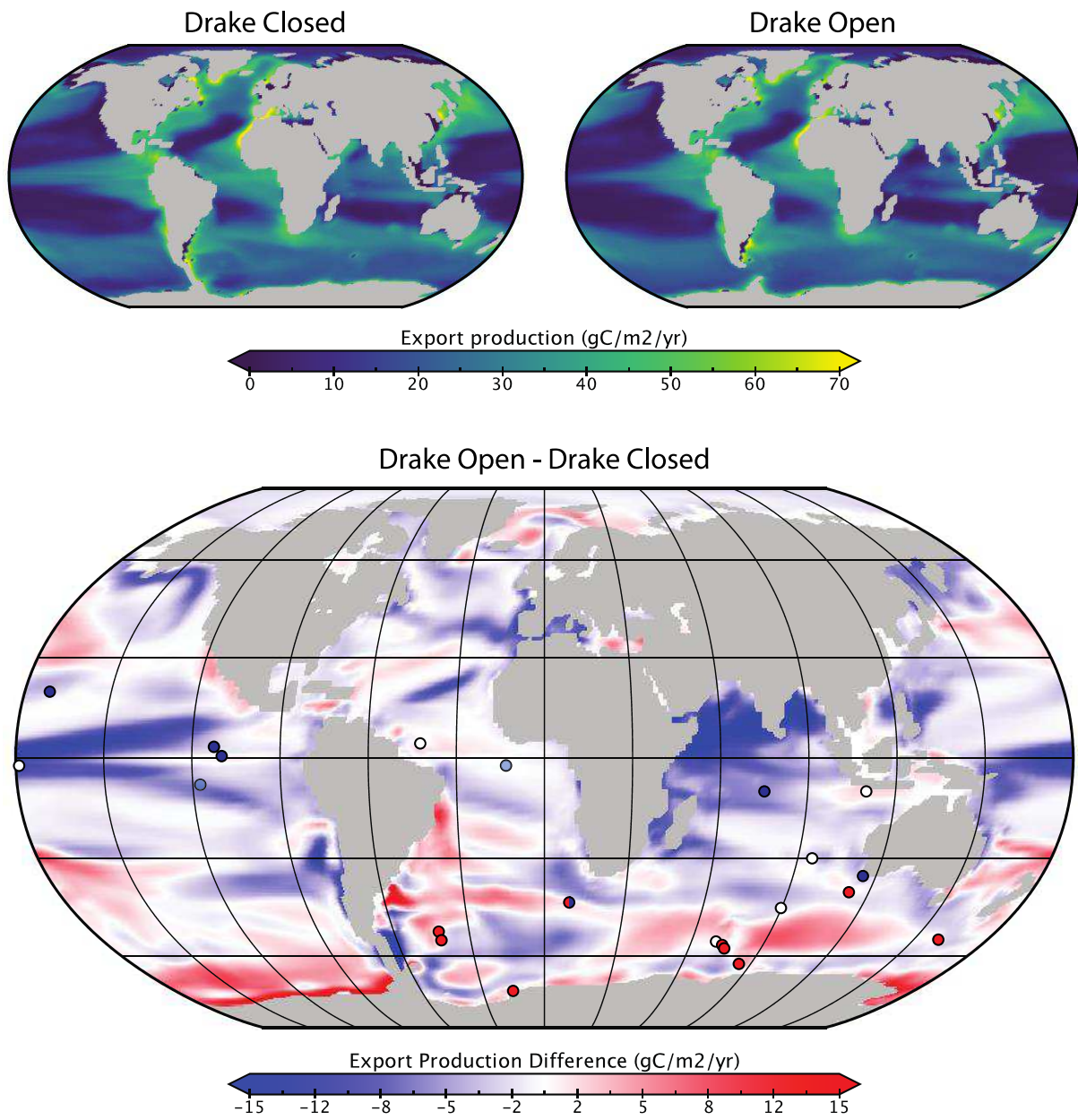


Figure 1.

835

836

837

838

839

840

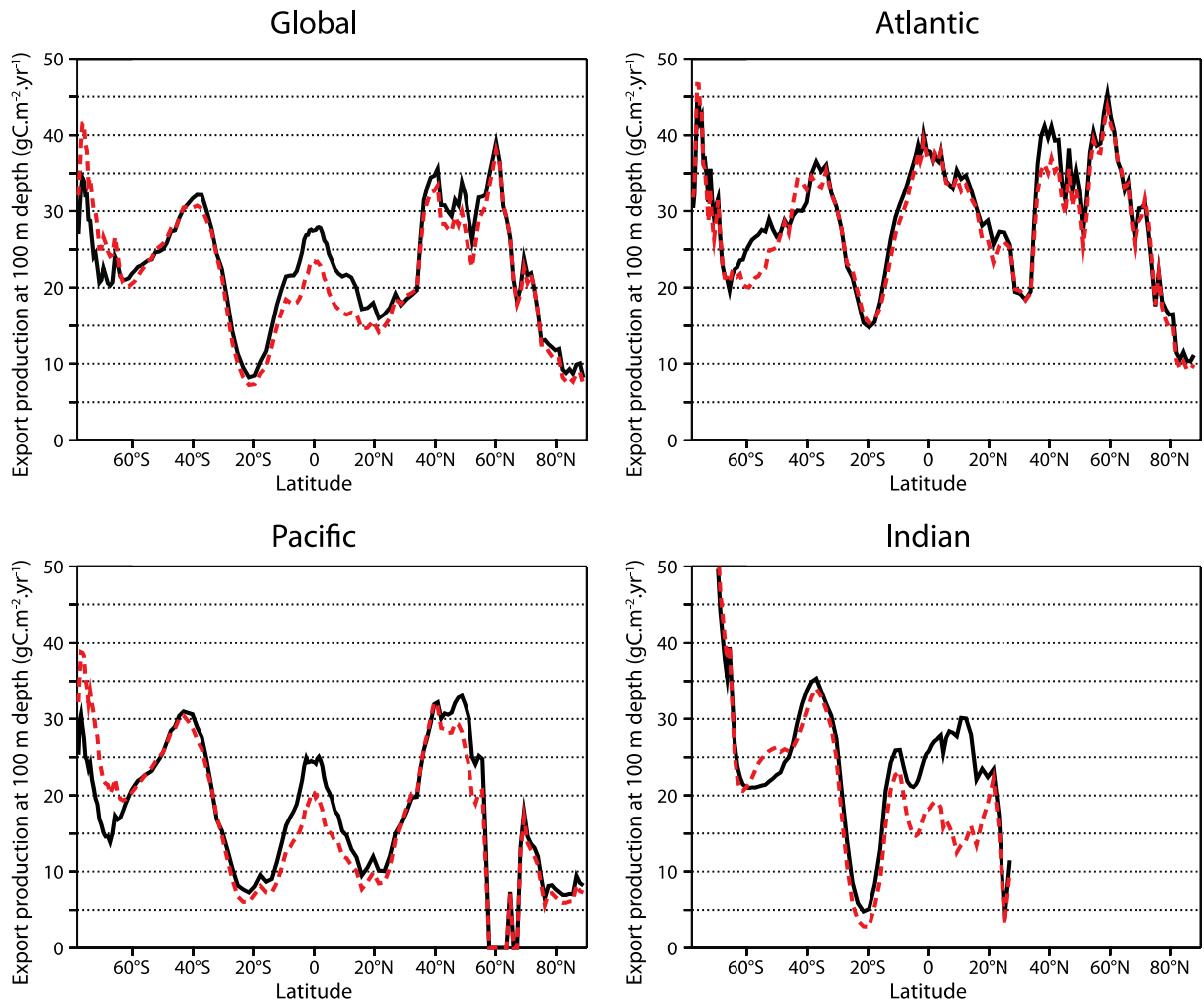


Figure 2.

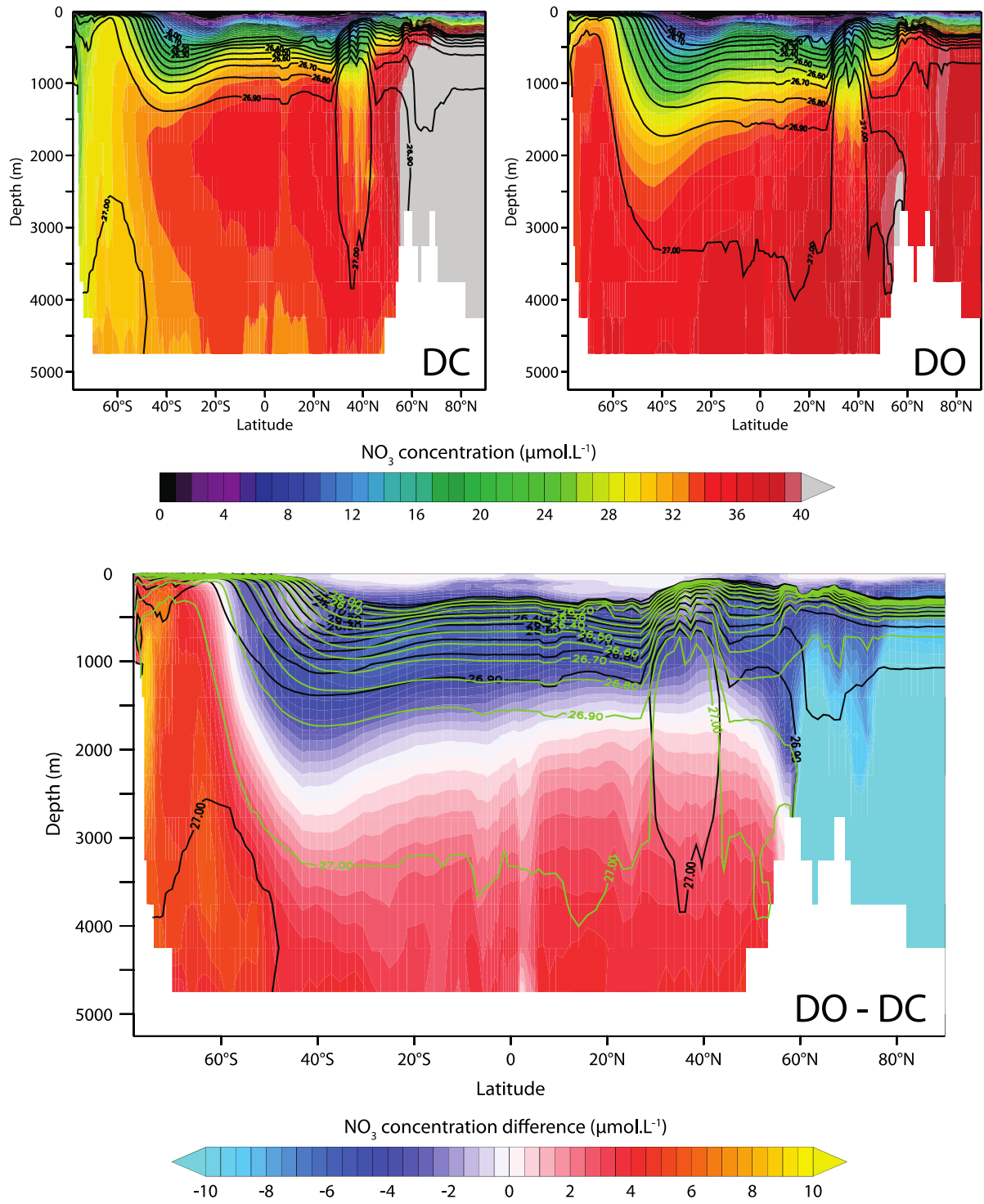


Figure 3.

842

843

844

845

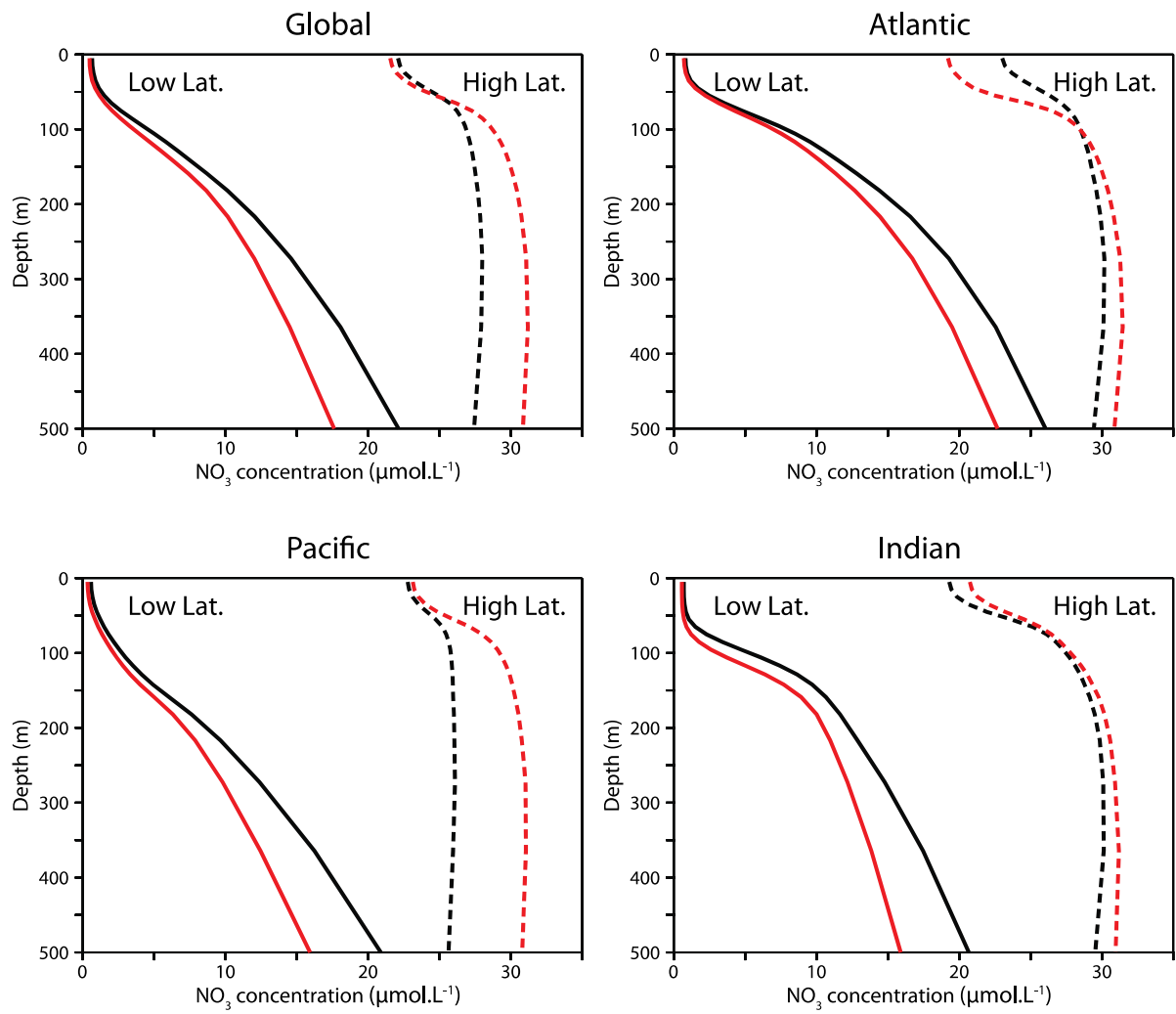


Figure 4.

846

847

848

849

850

851

852

853

854

855

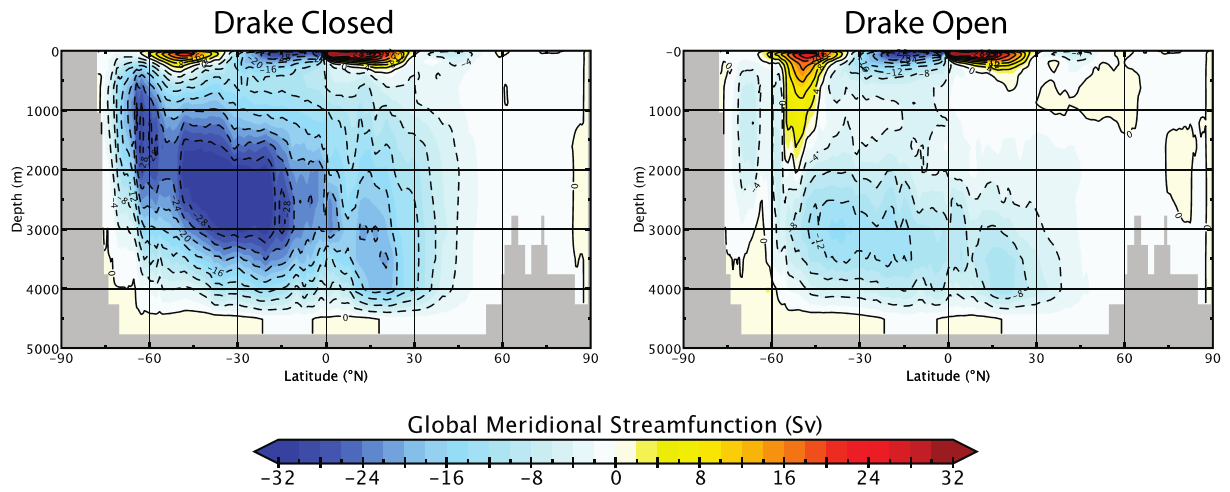


Figure 5.

856

857

858

859

860

861

862

863

864

865

866

867

868

869

870

871

872

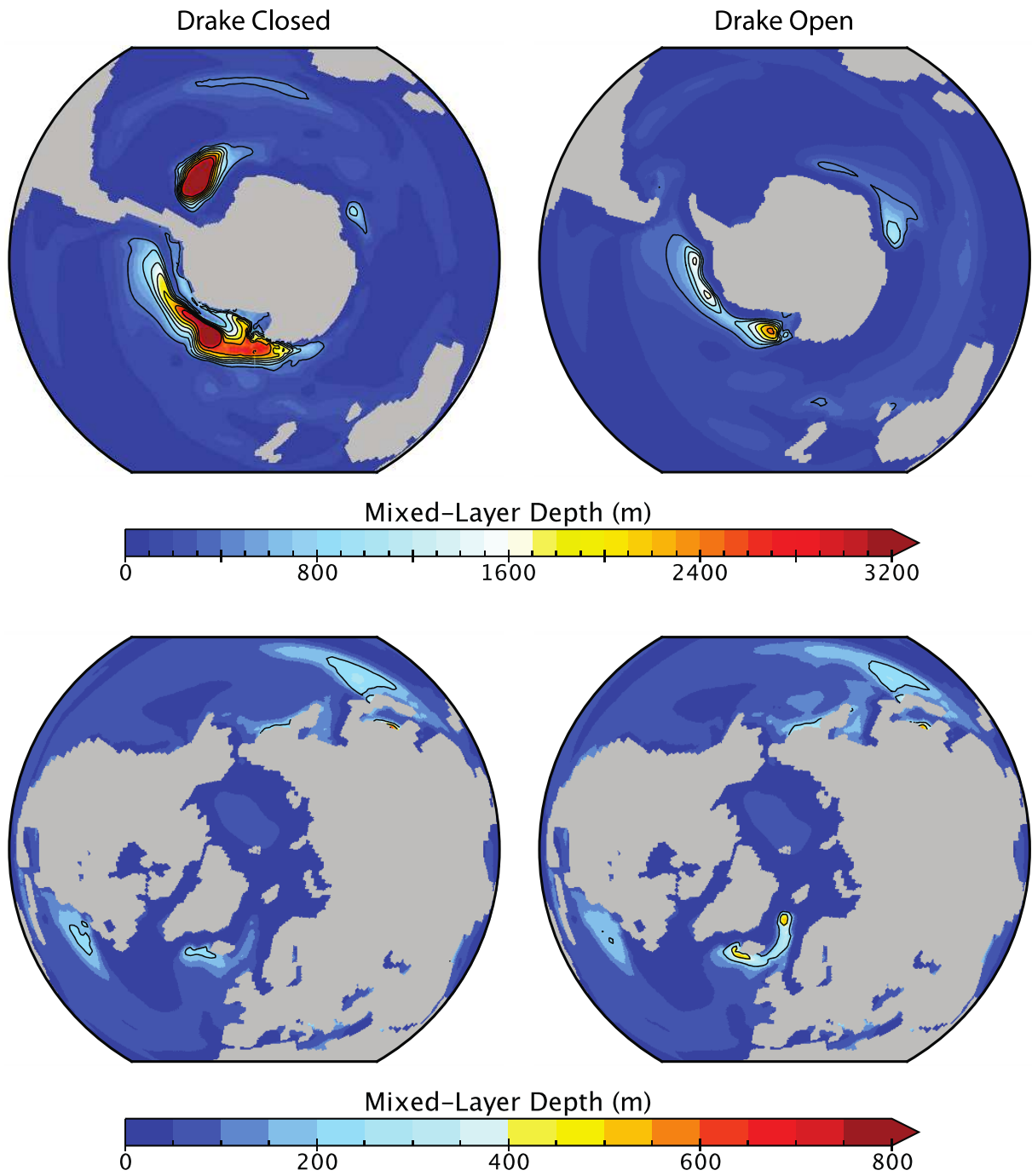


Figure 6.

873

874

875

876

877

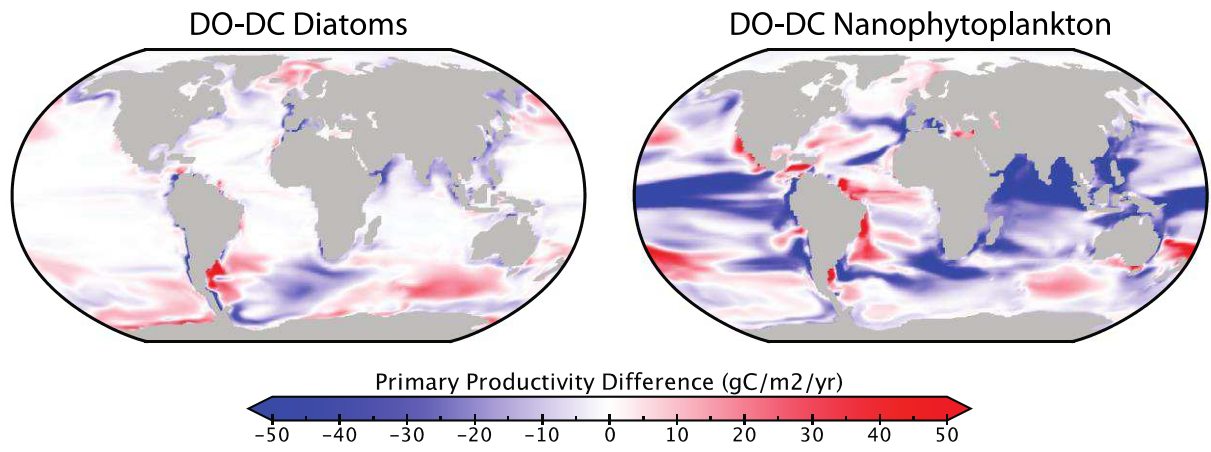


Figure 7.

878

879

880